

A non-repeating fast radio burst in a dwarf host galaxy

SHIVANI BHANDARI,^{1,2,3,*} ALEXA C. GORDON,⁴ DANICA R. SCOTT,⁵ LACHLAN MARNOCH,^{6,3,7,8} NAVIN SRIDHAR,^{9,10}
PRAVIR KUMAR,^{11,12} CLANCY W. JAMES,⁵ HAO QIU,¹³ KEITH W. BANNISTER,³ ADAM T. DELLER,¹¹
TARRANEH EFTEKHARI,^{4,†} WEN-FAI FONG,⁴ MARCIN GLOWACKI,⁵ J. XAVIER PROCHASKA,^{14,15,16,‡} STUART D. RYDER,^{6,7}
RYAN M. SHANNON,¹¹ AND SUNIL SIMHA¹⁴

¹*ASTRON, Netherlands Institute for Radio Astronomy, Oude Hoogeveensedijk 4, 7991 PD Dwingeloo, The Netherlands*

²*Joint institute for VLBI ERIC, Oude Hoogeveensedijk 4, 7991 PD Dwingeloo, The Netherlands*

³*CSIRO, Space and Astronomy, PO Box 76, Epping NSW 1710 Australia*

⁴*Center for Interdisciplinary Exploration and Research in Astrophysics (CIERA) and Department of Physics and Astronomy, Northwestern University, Evanston, IL 60208, USA*

⁵*International Centre for Radio Astronomy Research (ICRAR), Curtin University, Bentley, WA 6102, Australia*

⁶*School of Mathematical and Physical Sciences, Macquarie University, NSW 2109, Australia*

⁷*Astronomy, Astrophysics and Astrophotonics Research Centre, Macquarie University, Sydney, NSW 2109, Australia*

⁸*ARC Centre of Excellence for All-Sky Astrophysics in 3 Dimensions (ASTRO 3D), Australia*

⁹*Department of Astronomy, Columbia University, New York, NY 10027, USA*

¹⁰*Theoretical High Energy Astrophysics (THEA) Group, Columbia University, New York, NY 10027, USA*

¹¹*Centre for Astrophysics and Supercomputing, Swinburne University of Technology, John St, Hawthorn, VIC 3122, Australia*

¹²*Department of Particle Physics and Astrophysics, Weizmann Institute of Science, Rehovot 7610001, Israel*

¹³*SKA Observatory, Jodrell Bank, Lower Withington, Macclesfield, SK11 9FT, UK*

¹⁴*University of California - Santa Cruz 1156 High St. Santa Cruz, CA, USA 95064*

¹⁵*Kaoli IPMU (WPI), UTIAS, The University of Tokyo, Kashiwa, Chiba 277-8583, Japan*

¹⁶*Division of Science, National Astronomical Observatory of Japan, 2-21-1 Osawa, Mitaka, Tokyo 181-8588, Japan*

ABSTRACT

We present the discovery of as-of-yet non-repeating Fast Radio Burst (FRB), FRB 20210117A, with the Australian Square Kilometer Array Pathfinder (ASKAP) as a part of the Commensal Real-time ASKAP Fast Transients (CRAFT) Survey. The sub-arcsecond localization of the burst led to the identification of its host galaxy at a $z = 0.214(1)$. This redshift is much lower than what would be expected for a source dispersion measure (DM) of 729 pc cm^{-3} , given typical contributions from the intergalactic medium and the host galaxy. Optical observations reveal the host to be a dwarf galaxy with little on-going star formation, very different to the dwarf host galaxies of known repeating FRBs 20121102A, and 20190520B. We find an excess DM contribution from the host and attribute it to the FRB's local environment. We do not find any radio emission from the FRB site or host galaxy. The low magnetized environment and lack of a persistent radio source (PRS) indicate that the FRB source is older than those found in other dwarf host galaxies, and establish the diversity of FRB sources in dwarf galaxy environments. We find our observations to be fully consistent with the hypernebula model, where the FRB is powered by accretion-jet from a hyper-accreting black hole. Finally, our high-time resolution analysis reveals burst characteristics similar to those seen in repeating FRBs. We encourage follow-up observations of FRB 20210117A to establish any repeating nature.

Keywords: radio continuum: general, instrumentation: interferometers, galaxies: star formation

1. INTRODUCTION

Corresponding author: Shivani Bhandari
bhandari@astron.nl

‡ Simons Pivot Fellow

* Veni fellow

† NHFP Einstein Fellow

Fast radio bursts (FRBs) are nano- to milli-second duration pulses of coherent radio emission with dispersion measures (DM) exceeding the maximum expected contribution from the Milky Way along a given line of sight (Petroff et al. 2016). The majority of the published sample of > 600 FRBs are dominated by non-repeating events; only 4% of FRB sources are observed to emit repeating bursts (Amiri et al. 2021). While the fundamental relationship between repeating and non-repeating FRBs is unknown, the growing sample reveals statistical differences in the burst properties of the two speculative populations (Pleunis et al. 2021). There are, however, no significant differences between the galaxies hosting repeating and non-repeating FRBs (Bhandari et al. 2022). The localized sample of 22 FRBs mostly comes from the outskirts of their host galaxies at redshifts ranging from less than 0.001 to 1.016 and have diverse host and local environments (Tendulkar et al. 2017; Ravi et al. 2019; Marcote et al. 2020; Bhandari et al. 2020; Heintz et al. 2020; Fong et al. 2021; Niu et al. 2022; Bhandari et al. 2022; Kirsten et al. 2022; Ryder et al. 2022; Ravi et al. 2022).

The first repeating FRB 20121102A (Spitler et al. 2016) is localized to a low-metallicity dwarf host galaxy with a high specific star formation rate at $z = 0.192$ (Tendulkar et al. 2017). The burst was found to be co-located with a compact persistent radio source (PRS; < 0.7 pc in size) suggesting that the FRB source is embedded in a radio nebula (Chatterjee et al. 2017; Marcote et al. 2017). Also, the repeat bursts were observed to have exceptionally high ($\sim 10^5$ rad m $^{-2}$) and highly variable rotation measure (Michilli et al. 2018; Hilmarsen et al. 2021). The properties of the local environment and host galaxy of FRB 20121102A led to a concordant model for FRBs in which bursts are produced by young magnetars, themselves produced in superluminous supernovae or long gamma-ray bursts (Margalit & Metzger 2018). Alternatively, the PRS can also be self-consistently explained by an accreting compact object engine (Sridhar & Metzger 2022; Chen et al. 2022).

More recently, the repeating FRB 20190520B was discovered using the FAST radio telescope. The observed DM of 1202 pc cm $^{-3}$ would imply a redshift of $z \gtrsim 1$ (Macquart et al. 2020). Surprisingly, however, the localization of the FRB and optical observations revealed a dwarf host galaxy at $z = 0.241$, making this source the FRB with the highest host DM contribution of $DM_{\text{host}} = 903_{-111}^{+72}$ pc cm $^{-3}$ (Niu et al. 2022). This is unlikely to be due to the interstellar medium of the host galaxy, but rather more plausibly from the local environment of the source. This host DM is a factor of ~ 5 larger than what is observed for FRB host

galaxies (James et al. 2022b) and a factor of a few beyond what is estimated for FRB 20121102A (Tendulkar et al. 2017). Interestingly, similar to FRB 20121102A, FRB 20190520B is co-located with a PRS (the second only ever to be found). Furthermore, these two FRBs are among the active repeating sources and are also linked with PRSs, implying that these may be the characteristics of young and active FRB sources surrounded by dense and magnetized plasma.

Alternatively, other FRBs have been found in massive and moderately star-forming galaxies lacking a strong magnetic environment and radio nebula. It is possible that such sources are relatively older or live in less dense environments leading to an underluminous PRS (Margalit et al. 2019; Sridhar & Metzger 2022). Also, a CHIME/FRB repeating source FRB 20200120E was recently localized to a globular cluster in the galaxy M81, revealing a very different local environment for this source (Kirsten et al. 2022).

It is appealing to explain the wide variety of FRB environments using a connected mechanism, which is typically attributed to either the source age or the source formation channel. In either case, a knowledge of the environment surrounding a larger sample of FRBs is the key to understanding this potential connection. The presence or absence of a PRS or radio emission from star formation, and how it correlates with FRB properties such as repetition rate, dispersion measure due to the host galaxy, rotation measures etc, is thus critical.

We present the discovery of the apparently non-repeating FRB 20210117A with the Australian Square Kilometre Array Pathfinder (ASKAP) and its localization to a dwarf galaxy in this paper. Section 2 describes the discovery as well as the properties of the host galaxy. Section 3 presents the high time resolution analysis of the burst. Section 4 describes radio follow-up observations made to look for a PRS and repeating bursts from the source of FRB 20210117A. Section 5 discusses the implications of our findings, and Section 6 provides a summary.

2. DISCOVERY OF FRB 20210117A

The burst was detected on 2021 January 17 UT 07:51:21.277 in the real-time CRAFT incoherent sum search observations using 26 ASKAP dishes at a centre frequency of 1271.5 MHz spanning a bandwidth of 336 MHz. These observations were carried out simultaneously with the Rapid ASKAP Continuum Survey (McConnell et al. 2020, RACS) observation. The burst, however, was not detected in a 10-s commensal ASKAP snapshot taken during a 15-minute RACS pointing. In CRAFT data, the burst had a maximum S/N of 27.1

in the outer ASKAP beam 02 and was also detected in beams 01 and 07, with S/N of 16.3 and 4.7 respectively, of the closepack36 beam footprint pattern (see [Shannon et al. 2018](#)). The burst has a fluence of 36_{-9}^{+28} Jy ms and a structure-maximized DM of $729.1_{-0.23}^{+0.36}$ pc cm⁻³, which is derived using the method described in [Sutinjo et al. \(2023\)](#). The k-corrected isotropic-equivalent spectral energy of the burst is derived using:

$$E_\nu = \frac{4\pi D_L(z)^2}{(1+z)^{2+\alpha}} F_\nu, \quad (1)$$

where $D_L(z)$ is luminosity distance, F_ν is burst fluence and α is the spectral index ($F \propto \nu^\alpha$) ([James et al. 2022a](#)). We use a default value of $\alpha = -1.5$ ([Macquart et al. 2019](#)) and derive $E_\nu = 4.6 \times 10^{31}$ erg Hz⁻¹. We note that any beaming of the FRB can reduce this energy budget by a factor of $\Delta\Omega/4\pi$, where $\Delta\Omega$ is the unknown beaming solid angle. Furthermore, if beaming is invoked to reduce the energy of a burst, it implies that such bursts are more numerous, as we only see a fraction of them. Other measured and derived properties of FRB 20210117A are listed in Table 1.

The detection in the real-time system triggered a download of 3.1s of voltages around the time of the FRB. Using the standard CRAFT post-processing pipeline ([Day et al. 2020](#)), we imaged both the FRB and the continuum sources visible in the field. The FRB was detected with a significance of 50σ , leading to a statistical positional precision of $\sim 0.1''$ in R.A. and Decl. We used the method described in [Day et al. \(2021\)](#) to estimate the systematic uncertainties by identifying 7 compact sources greater than 7σ in the 3-sec field image and comparing them to their counterparts in the RACS radio image. We obtain an offset correction of $0.02'' \pm 0.08''$ in R.A. and $0.01'' \pm 0.08''$ in Decl. The final burst position is R.A.(J2000): 22h39m55.015s and Decl.(J2000): $-16^\circ 09' 05.45''$ with an uncertainty of $0.13'' \times 0.12''$.

2.1. Host galaxy of FRB 20210117A

On 2021 June 10/11, we used the Keck/DEIMOS to image the field in r -band. The data revealed a faint galaxy with $r \sim 23$, coincident with the position of the burst. We performed a Probabilistic Association of Transient Hosts (PATH; [Aggarwal et al. 2021](#)) analysis which yielded a $P(O|x) = 0.9984$ posterior probability that this source is the host of FRB 20210117A.

On 2021 June 12 UT, additional imaging observations in the g - and I -bands were obtained with the FORS2 instrument mounted on Unit Telescope 1 (UT1) of the European Southern Observatory's Very Large Telescope (ESO VLT). The images were processed as described by

[Marnoch et al. \(2020\)](#): debiasing and flatfielding was carried out using ESOReflex¹ ([Freudling et al. 2013](#)); mosaicing with Montage² ([Berriman & Good 2017](#)); and astrometric calibration using a local installation of Astrometry.net³ ([Lang et al. 2010](#)) incorporating the Gaia ([Lindegren et al. 2018](#)) catalog; this results in a precision (calculated as the the RMS of the offsets of imaged stars from counterparts in Gaia DR3) of $\sim 0.07''$ for both bands. The g -band image was calibrated photometrically against DR2 of the DELVE catalogue ([Drlica-Wagner et al. 2022](#)), and the I -band using the FORS2 Quality Control archive. The total integration times and image quality were 5000/900 sec and 0.70/0.65 arc-sec in g/I , respectively. Further imaging was acquired on 2022 June 10 UT with the HAWK-I instrument, on UT4 of the ESO VLT, in J , H and K_s bands. ESOReflex was used for the debiasing, flatfielding and coaddition of the images, while photometric calibration was performed against the 2MASS Point-Source Catalog ([Skrutskie et al. 2006](#)). The astrometric calibration was performed using the same procedure as FORS2. Each band was observed for a total integration time of 750 seconds. See Table 1 for photometric details.

2.1.1. Host galaxy spectrum

Having identified the most likely host galaxy in these images (Fig. 1), follow-up spectroscopy using FORS2 with a $1''$ slit, the GRIS300I grism and OG590 order sorting filter was obtained on 2021 Sep 6 UT. This yielded wavelength coverage of 600–1100 nm at a resolution of 660. The total on-source exposure time was 2600 sec.

The spectrum was reduced with the Python Spectroscopic Data Reduction Pipeline (PypeIt; [Prochaska et al. 2020](#)). PypeIt performed flat-fielding, bias subtraction, wavelength calibration, and spectral extraction using the standard default parameters. The spectrum was then flux calibrated using the spectrophotometric standard star EG21 which was observed on 2021 Sep 2 UT. The two 1300s exposures were combined via 1D coaddition and scaled to match the Keck/DEIMOS r -band flux. Finally, the spectrum was telluric-corrected using the Paranal VIS 4900 atmospheric grid and corrected for extinction using the [Calzetti \(2001\)](#) extinction law. A detection of H α , [S II] doublet and [O III] doublet spectral lines confirmed the redshift of the host to be $z = 0.214(1)$. No other spectral lines are apparent in the data.

¹ <https://www.eso.org/sci/software/esoreflex/>

² <http://montage.ipac.caltech.edu/>

³ <http://astrometry.net/>

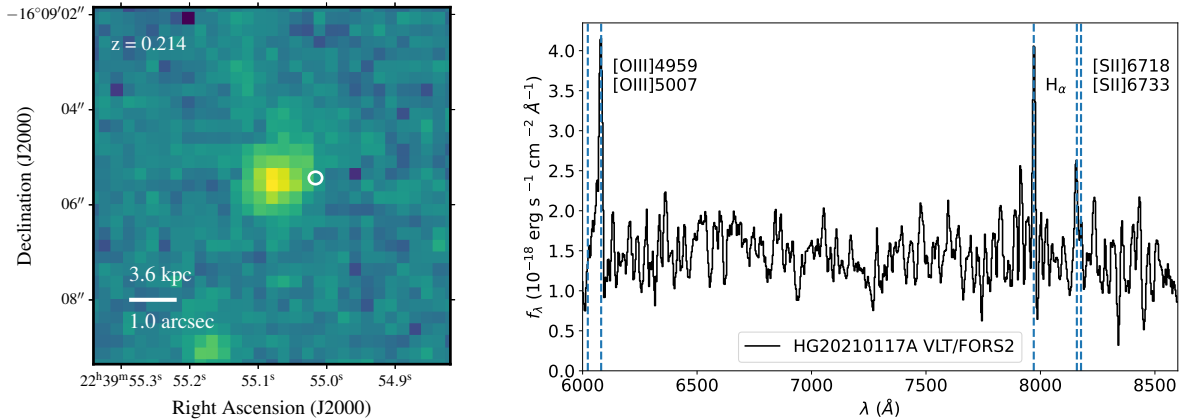


Figure 1. Left: I -band VLT/FORS2 image of the host galaxy of FRB 20210117A overplotted with the position of the burst. The white circle represents the total uncertainty (1σ) in the FRB position. Right: VLT/FORS2 spectrum of the FRB 20210117A host galaxy which is used to estimate the redshift of the host to be $z = 0.214$.

2.1.2. Stellar population modeling

To determine the stellar population properties of the host galaxy, the stellar population synthesis modeling code `Prospector` (Johnson et al. 2021) was used. The observed photometry and spectroscopy were jointly fit using the stellar population synthesis library `python-fsps` (Conroy et al. 2009; Conroy & Gunn 2010). We assume a Kroupa initial mass function (IMF) Kroupa (2001) and Kriek & Conroy (2013) dust attenuation curve. Additional assumed priors include a ratio on dust attenuation between old and young stars, mass-metallicity relationship (Gallazzi et al. 2005), and a continuity non-parametric star formation history (SFH, Leja et al. (2019)) using 8 age bins. Several spectroscopic calibration parameters were used including a spectral smoothing parameter, a parameter to normalize the spectrum to the photometry, a pixel outlier model to marginalize over poorly modeled noise, and a jitter model to inflate the noise in all spectroscopic pixels to

ensure a better fit between the model and observed spectrum. A 12th order Chebyshev polynomial was then used to fit the spectral continuum. Our assumed model, as described above, was then sampled using the dynamic nested sampling routine `dynesty` (Speagle 2020) to produce the posterior distributions of stellar population parameters.

The resulting model reveals a dwarf galaxy with a stellar mass of $\log(M_*/M_\odot) = 8.56^{+0.06}_{-0.08}$ and mass-weighted age of $5.06^{+0.91}_{-1.34}$ Gyr (Gordon et al 2023., in prep.), a metric less biased by the youngest and brightest stars in the galaxy compared to traditional light-weighted ages (Conroy 2013). The host has a low current star formation rate (SFR) with an average SFR over the past 100 Myr of $0.014^{+0.008}_{-0.004} M_\odot \text{ yr}^{-1}$. These values and other host properties are reported in Table 1. We note that as `prospector` is a Bayesian inference code, the uncertainties on the stellar parameters correspond to the 68% confidence intervals on the posteriors, given all of the priors for the assumed model.

Table 1. Measured and derived properties FRB 20210117A and its host galaxy.

Measured burst properties	
Arrival time at 1271.5 MHz	2021-01-17-07:51:21.277
S/N	27.0
Structure-maximized DM (pc cm^{-3})	$729.1^{+0.36}_{-0.23}$
DM _{ISM} NE2001 (pc cm^{-3})	34
DM _{ISM} YMW16 (pc cm^{-3})	23
DM _{cosmic} (pc cm^{-3})	~ 184

Table 1 continued

Table 1 (*continued*)

DM_{host} (pc cm ⁻³)	~ 460
RA (J2000)	22h39m55.015(9)s
Dec (J2000)	$-16^{\circ}09'05.45(12)''$
Fluence (Jy ms)	36_{-9}^{+28}
Peak1 pulse width (ms)*	0.14 ± 0.01
Peak2 pulse width (ms)*	0.17 ± 0.02
Precursor component pulse width (ms)*	0.53 ± 0.03
Scattering time ($\tau_{1.2\text{GHz}}$) (ms)	0.33 ± 0.02
Rotation measure (RM) (rad m ⁻²)	43 ± 0.6
Spectral energy density (erg Hz ⁻¹)	4.6×10^{31}
PRS luminosity ($L_{6\text{GHz}}$) (W Hz ⁻¹)	$< 1.5 \times 10^{21}$
Host galaxy properties	
RA (J2000)	22h39m55.07(2)s
Dec (J2000)	$-16^{\circ}09'05.37(2)''$
Redshift	0.214(1)
g (AB mag)	23.60 ± 0.02
r (AB mag)	22.97 ± 0.04
I (AB mag)	22.23 ± 0.05
J (AB mag)	22.69 ± 0.08
H (AB mag)	22.94 ± 0.1
K (AB mag)	22.80 ± 0.1
$u - r$ (restframe)	1.0 ± 0.1
M_r (restframe)	-17.23 ± 0.05
$\log(M_*/M_{\odot})$	$8.56_{-0.08}^{+0.06}$
100 Myr SFR ($M_{\odot} \text{ yr}^{-1}$)	$0.014_{-0.004}^{+0.008}$
$\log(\text{sSFR})$ (yr ⁻¹)	-10.4
Mass-weighted age (Gyr)	$5.06_{-1.34}^{+0.91}$
Projected offset from galaxy center (kpc)	2.8 ± 0.4

* Reported widths are 1σ of the Gaussian

2.2. Excess host DM

The observed DM of the FRB can be divided into contributions from various components as

$$DM_{\text{obs}} = DM_{\text{MW,ISM}} + DM_{\text{MW,halo}} + DM_{\text{EG}} \quad (2)$$

$$DM_{\text{EG}} = DM_{\text{cosmic}} + \frac{DM_{\text{host}}}{1+z}.$$

Here $DM_{\text{MW,ISM}}$ and $DM_{\text{MW,halo}}$ are the contributions due to the Milky Way's interstellar medium and halo. These are estimated to be 34 pc cm^{-3} and 23 pc cm^{-3} from the Galactic models of NE2001 (Cordes & Lazio 2002) and YMW16 (Yao et al. 2017), respectively and $DM_{\text{MW,halo}}$ is assumed to be 50 pc cm^{-3} (Prochaska & Zheng 2019). DM_{EG} refers to the extragalactic DM which is composed of the contributions due to the IGM/foreground halos along the FRB sight-

line (DM_{cosmic}) and the host galaxy of FRB (DM_{host}). DM_{cosmic} is estimated to be 183 pc cm^{-3} using the Macquart (DM-z) relation (Macquart et al. 2020). After subtracting the respective contributions from the Milky Way (using NE2001) and IGM from the observed DM of the FRB, we find DM_{host} to be $\sim 460 \text{ pc cm}^{-3}$, which is greater than what has been observed for ASKAP-localized FRBs (a median of $DM_{\text{host}} = 186_{-48}^{+59} \text{ pc cm}^{-3}$ (James et al. 2022b)). A much lower value is possible if the sightline exhibits a higher DM_{cosmic} value than typical; see Simha et al. (in prep) for such a test hypothesis. When we include the variation in DM_{cosmic} from Macquart et al. (2020) with a feedback parameter $F = 0.32$ into Eq. 2, we produce a distribution for DM_{host} . Scaling this to the host galaxy rest frame by $1+z$ as per Ryder et al. (2022) produces Figure 2, where the rest-frame DM is compared to other FRBs with large DM_{host} contributions. Using this method, we estimate

the median rest-frame DM_{host} for FRB 20210117 to be $595_{-24}^{+55} \text{ pc cm}^{-3}$.

James et al. (2022a) demonstrated that it is critical to consider observational biases in a survey because they can result in an inversion of the Macquart relationship after a certain DM value. Using their $P(DM_{\text{EG}}, z)$ grid for the CRAFT/ICS survey, we calculate the probability distribution function (pdf), $P(DM_{\text{EG}} | z)$, given the redshift of FRB 20210117A. The pdf is presented in Fig. 3, which reaches its maximum at an extragalactic DM of 182 pc cm^{-3} , with 1σ confidence interval spanning $176 - 496 \text{ pc cm}^{-3}$. We also show the pdf of the DM due to the IGM and the extragalactic DM, both of which are free of any instrumental biases.

The host DM contribution can be probed by optical studies. We use the $H\alpha$ flux measurement from the spectrum of the host to constrain host DM. We measure $F_{H\alpha} = 1.7 \times 10^{-17} \text{ erg cm}^{-2} \text{ s}^{-1}$ and use it to derive the $H\alpha$ luminosity of $L_{H\alpha} = 2.3 \times 10^{39} \text{ erg s}^{-1}$. Dwarfs of the Magellanic type range in size from 1 to 5 kpc (Kaisin et al. 2012). For simplicity, we assume the size of the dwarf host galaxy to be 3 kpc as we are unable to fit a sersic profile due to galaxy’s unresolved nature. Thirdly, $H\alpha$ luminosity is proportional to $\int n_e^2 dV$ because it is a tracer of ionized hydrogen, implying that the free electron density is proportional to the square root of the total $H\alpha$ luminosity emitted by the host galaxy, $n_e \propto \sqrt{L_{H\alpha}/V}$ (Xu & Han 2015), where V is the volume of a sphere. We note that this assumes the volume of galaxies like the MW and dwarfs are uniformly ionized. According to statistics of Milky Way-type galaxies (James et al. 2004), the total $L_{H\alpha}$ from the Milky Way is $\sim 10^{40} \text{ erg s}^{-1}$, and the size of the MW is 30 kpc. Finally, using the above relation, we obtain,

$$\frac{n_{e,\text{host}}}{n_{e,\text{MW}}} \propto \sqrt{\frac{L_{H\alpha,\text{host}}/V_{\text{host}}}{L_{H\alpha,\text{MW}}/V_{\text{MW}}}},$$

$$\frac{DM_{\text{host}}}{DM_{\text{MW}}} = \frac{n_{e,\text{host}}}{n_{e,\text{MW}}} \cdot \frac{l_{\text{host}}}{l_{\text{MW}}},$$

$$DM_{\text{host}} \propto DM_{\text{MW}} \left(\frac{L_{H\alpha,\text{host}}}{L_{H\alpha,\text{MW}}} \right)^{1/2} \left(\frac{R_{\text{MW}}}{R_{\text{host}}} \right)^{3/2} \left(\frac{l_{\text{host}}}{l_{\text{MW}}} \right). \quad (3)$$

Here l_{host} and l_{MW} are the path lengths along the host and the Milky Way, which are assumed to be twice the effective radius of the galaxy. Using the DM_{MW} contribution from NE2001, we estimate DM_{host} to be $\sim 60 \text{ pc cm}^{-3}$. We are unable to estimate the host’s inclination angle because the galaxy is barely resolved in our observations. Nevertheless, we note that in a simulation to model the DM due to dwarf galaxies, Xu & Han (2015) find the DM to be $11 - 12 \text{ pc cm}^{-3}$,

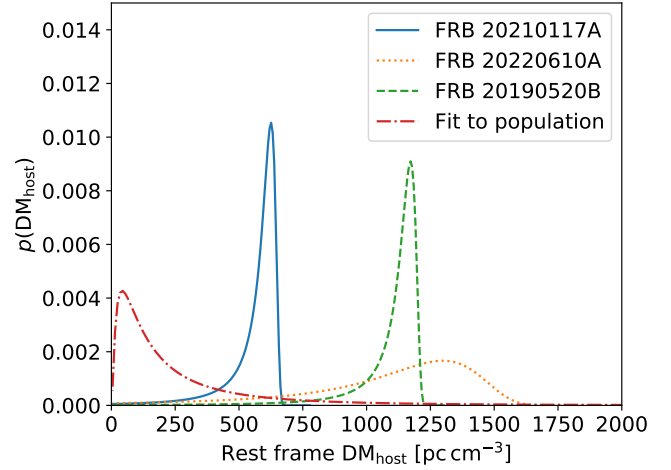


Figure 2. Probability density functions $P(DM_{\text{host}})$ for the host galaxy DM contribution, scaled by $1 + z$ to the host galaxy’s rest frame. Shown are values for three localized FRBs — blue solid: FRB 20210117; green dashed: FRB 20190520B (Niu et al. 2022); orange dotted: FRB 20220610A (Ryder et al. 2022) — and the log-normal fit to the FRB population based on ASKAP and Parkes (Murriyang) data (James et al. 2022a).

$22 - 24 \text{ pc cm}^{-3}$, and about 100 pc cm^{-3} for inclination angles of 0, 60, and 90 degrees respectively. Thus, we conclude that the host ISM alone cannot dominate the excess DM observed along the FRB sightline, and that the excess DM must come from the local environment of FRB 20210117A.

3. HIGH-TIME RESOLUTION STUDIES

Using the CRAFT voltage data, we performed a high-time resolution analysis of the FRB. The data were beam-formed (coherently summed) at the position of the burst using the delay, bandpass, and phase solutions derived from the calibrator source PKS 0407–658. The 336 1-MHz bandwidth ASKAP channels containing FRB signal were then coherently de-dispersed at the FRB’s structure-maximized DM and passed through a synthesis filter to reconstruct a single 336-MHz channel with $\sim 3 \text{ ns}$ time resolution. Cho et al. (2020) provides a detailed description of the high time resolution construction process.

Next, we characterise the spectral modulation in the burst, which could be intrinsic to the burst emission, or be caused by propagation effects. The autocorrelation function (ACF) of the main component of the burst spectra $S(\Delta\nu)$ with a frequency resolution of 1 MHz is calculated as follows:

$$A(\delta\nu) = \frac{1}{N} \sum_{\nu} \Delta S(\nu) \Delta S(\nu + \delta\nu), \quad (4)$$

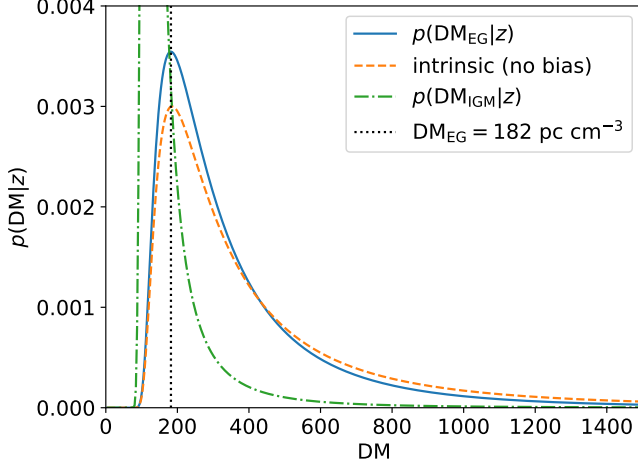


Figure 3. Probability density function (pdf) $P(\text{DM}_{\text{EG}} | z)$ for the extragalactic contribution to the DM given the redshift of the FRB host galaxy. The ASKAP ICS survey yields a blue curve after accounting for various survey biases (peak shown by vertical dashed line). The green curve represents the pdf of the DM due to the IGM only (i.e. without the host galaxy), and the orange curve the extragalactic DM free of instrumental biases.

where $\Delta S(\nu) = S(\nu) - \bar{S}$, \bar{S} is the mean spectral power and N is the number of frequency bins (Salpeter 1966). The ACF was then normalised by its maximum and fitted with a one-component Gaussian function from the `lmfit` python package. The central peak Full-Width at Half Maximum (FWHM) is 103 ± 4 MHz which is the characteristic frequency scale seen on the spectrum of burst’s main component. The fitted Gaussian function is then subtracted from the ACF, and the residuals are fitted with a Lorentzian function of the following form:

$$f(\delta\nu) = C \left(1 + \frac{\delta\nu^2}{\delta\nu_d^2} \right)^{-1}, \quad (5)$$

where C is a constant and $\delta\nu_d$ is the scintillation bandwidth (see Fig 4). We estimate $\delta\nu_d \sim 6$ MHz, which is consistent with the expectations for diffractive scintillation (DISS) from the Milky Way along the burst line of sight using the NE2001 model (~ 3 MHz at 1 GHz).

We fit the frequency-averaged pulse profile with scatter broadened Gaussian pulse models using nested sampling presented in Qiu et al. (2020) and Cho et al. (2020). This allows the fitting of multiple pulse components within the spectrum as demonstrated in Day et al. (2020).

We model the burst using a three-component scattered pulse with a precursor component (see Figure 5). Fitting of the averaged pulse profile gives a scattering time of $\tau = 0.33 \pm 0.02$ ms at centre frequency

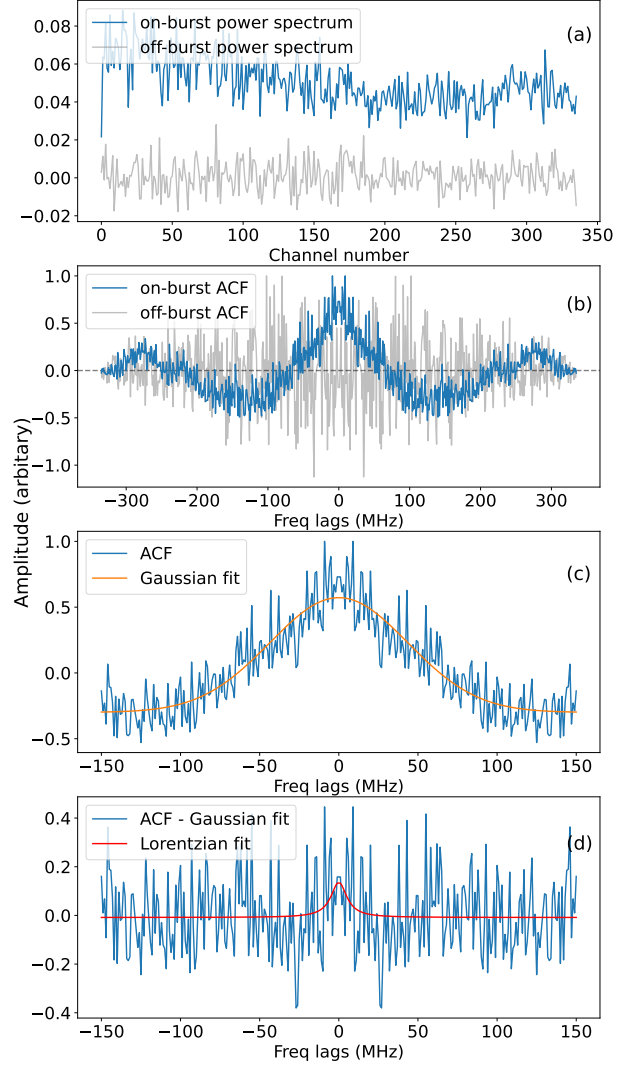


Figure 4. Autocorrelation function (ACF) analysis of the time-averaged spectrum of the FRB (resolution = 1 MHz). Panel (a) shows the burst on and off-peak power spectrum. On and Off-peak ACF function is shown in the panel (b). The noise spike with zero lag has been removed. A zoomed-in peak of the ACF fitted with a one-component Gaussian function is shown in panel (c). Panel (d) shows the Lorentzian fit to the residual.

of 1271 MHz, assuming $\tau \propto \nu^{-4}$. We note that the scattering fit was performed on the dynamic spectra dedispersed at the structure-maximized DM. We also estimate scattering time as a function of different DM trials between $728.6 - 729.4$ pc cm^{-3} and find a gradient of $-76 \mu\text{s}$ per pc cm^{-3} . We note that the scattering timescale is not consistent with the MW ($0.06 \mu\text{s}$ at 1 GHz) estimate from NE2001 model. Peak 1 and peak 2 have widths of 0.14 ± 0.01 ms and 0.17 ± 0.02 ms, respectively. The two peaks of the main pulse are separated by 0.60 ms. The precursor emission peak occurs

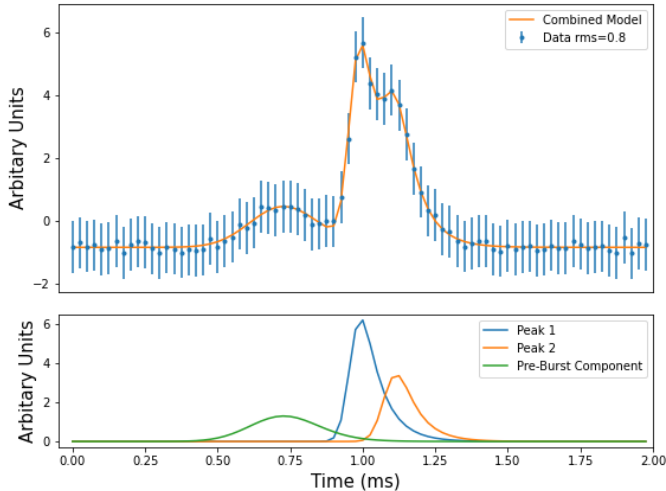


Figure 5. Pulse morphology model plot over 125 μs time series. The best-fit model comprises a scattered three component pulse profile .

~ 1.5 ms before the main peak with a pulse width of 0.53 ± 0.03 ms.

3.1. Polarimetry

The FRB data were polarisation calibrated using an observation of the Vela pulsar (PSR J0835–4510), which was observed 3.4 hr after the detection of the FRB. This ASKAP observation was compared to a Parkes radio telescope observation of the Vela pulsar with an accurate polarisation calibration to determine ASKAP’s instrumental leakage parameters (differential gain and phase between the two linearly polarized receptors), which were then applied to the burst data set. See Day et al. (2021) for additional details.

We used the RMFIT program in PSRCHIVE to calculate the rotation measure (RM) of FRB 20210117A and find the burst RM to be $43 \pm 0.6 \text{ rad m}^{-2}$. The frequency-integrated burst profiles (corrected for Faraday rotation) and the dynamic spectra are presented for all four Stokes parameters, in Figures 6 and 7 respectively. We see a hint of downward drifting structure in the dynamic spectrum, which has now been established as a distinguishing feature of repeating FRBs (Pleunis et al. 2021). Next, we use the method described in §2.4.1 of Day et al. (2020) to calculate the polarisation position angle (PA) Ψ and the associated uncertainty σ_Ψ , which was estimated using the Faraday-corrected Stokes profiles I , Q , and U . The uncertainties σ_I , σ_Q , and σ_U were estimated by taking the standard deviation of the off-burst Stokes I , Q , and U data. The PA and associated error is shown in the top panel of Fig 6.

We also calculate polarisation fractions for FRB 20210117A time window of 3.6 ms using the cal-

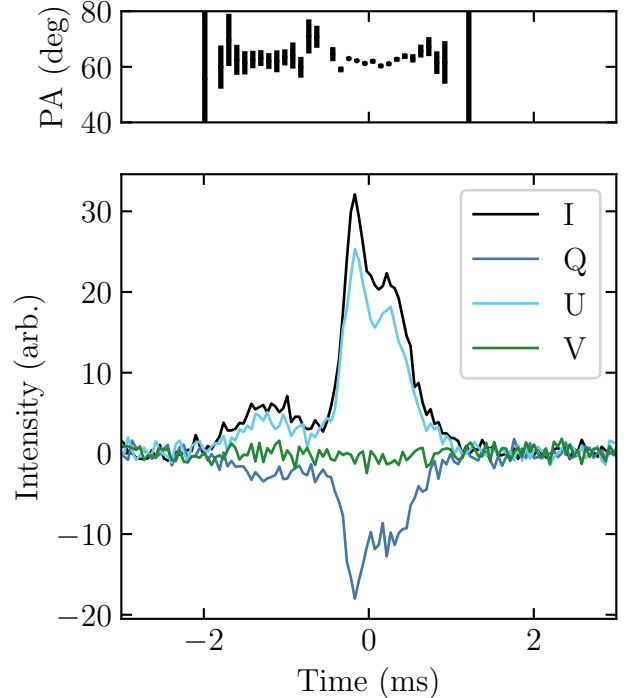


Figure 6. Faraday-corrected profiles of FRB20210117A. Top: polarisation position angle at a time resolution of 96 μs . Bottom: Stokes profiles at a time resolution of 48 μs .

ibrated Stokes parameters. The total de-bias linear polarisation and total polarisation is given by:

$$L_{\text{de-bias}} = \begin{cases} \sigma_I \sqrt{\left(\frac{L_{\text{meas}}}{\sigma_I}\right)^2 - 1} & \text{if } \frac{L_{\text{meas}}}{\sigma_I} > 1.57 \\ 0 & \text{otherwise.} \end{cases} \quad (6)$$

$$P = \sqrt{L_{\text{de-bias}}^2 + V^2} \quad (7)$$

Here, $L_{\text{meas}} = \sqrt{Q^2 + U^2}$. We obtain $L_{\text{de-bias}}/I = 0.90$, $V/I = -0.03$ and $P/I = 0.90$.

4. FOLLOW-UP RADIO OBSERVATIONS

4.1. Search for a radio persistent source

We observed the FRB field with the Karl G. Jansky Very Large Array (VLA) under the project code VLA/20B-103 on 2021 February 20. The source was observed for 52 minutes in 4 – 8 GHz frequency band centered at 6 GHz. We also conducted second epoch of follow-up observation with the Australia Compact Array Telescope (ATCA) on 2021 September 10 for ~ 3 hrs centered at 5.5 GHz and 7.5 GHz. We found no radio emission from anywhere in the host galaxy and no compact persistent radio source at the position of the burst. Our 3σ luminosity limits are $1.5 \times 10^{21} \text{ W Hz}^{-1}$ at 6 GHz

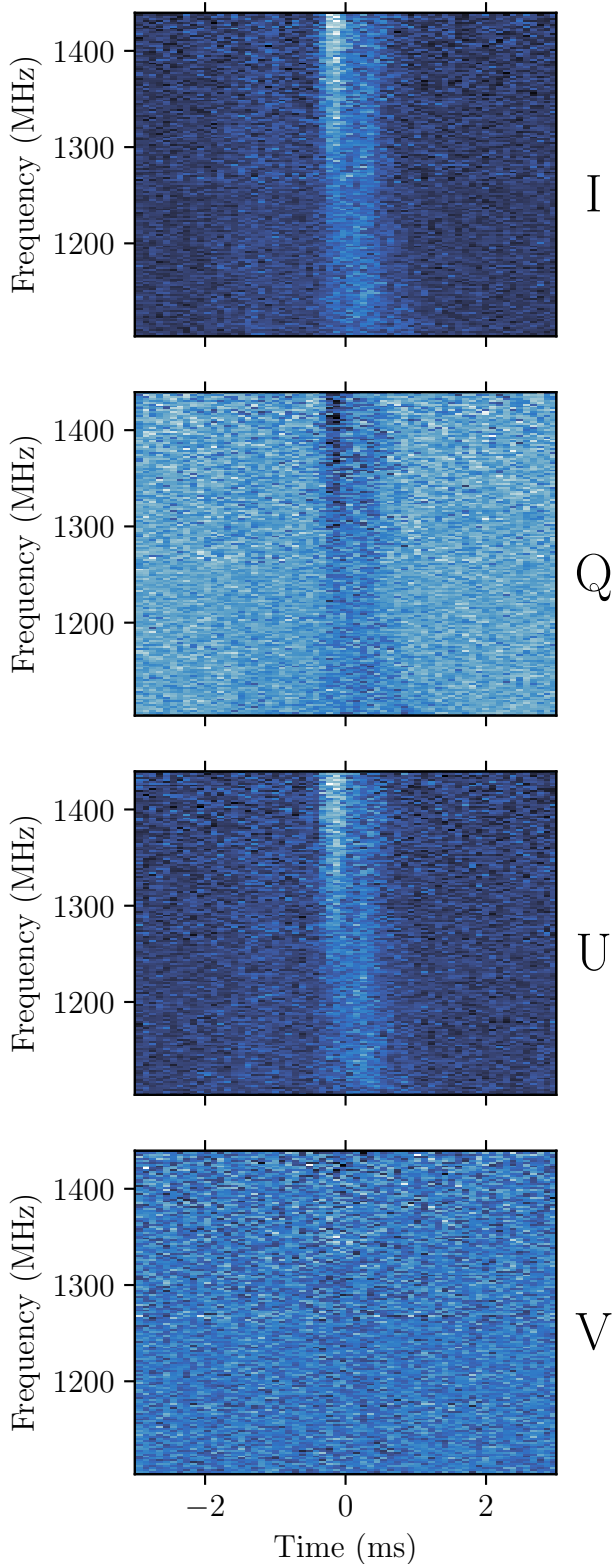


Figure 7. Faraday-corrected Stokes dynamic spectra of FRB20210117A at a time resolution of $96 \mu\text{s}$ and frequency resolution of 2 MHz.

and $4.0 \times 10^{21} \text{ W Hz}^{-1}$ at 6.5 GHz for both epochs respectively. These limits are lower than the luminosity of the FRB 2021102A PRS (see Table 2), indicating that FRB 20210117A may be an older source or in a less dense environment.

4.2. Search for repeating bursts

We conducted follow-up observations of FRB 20210117A using the ultra-wideband low (UWL) receiver at the 64-m Parkes radio telescope (also known as *Murriyang*). The observations were centred at 2368 MHz, with the bandwidth spanning 0.7 – 4 GHz. The FRB source was observed for a total of 9.2 hours during January and October 2021. We searched the Parkes data for repeat bursts and single pulses using the `Heimdall` (Barsdell 2012) and `Fetch` (Agarwal et al. 2020) software packages for a DM range of 100–1100 pc cm^{-3} , utilizing a tiered sub-band strategy as described in Kumar et al. (2021). No significant single-pulse candidates of astrophysical origin were identified in these observations above an S/N of 8. We can constrain the detectable fluence of the repeat bursts to be $\lesssim 0.15 \text{ Jy ms}$ in these UWL observations assuming a broadband pulse (3.3 GHz bandwidth) pulses with a nominal width of 1 ms. If the repeat bursts are narrowband (64 MHz bandwidth), in that case, our search pipeline was sensitive up to $\sim 1 \text{ Jy ms}$. Furthermore, the source was self-followed up with ASKAP between September 2021 to January 2022 for a duration of 125.53 hours, with the band centre frequency ranging from 920.5–1632.5 MHz. No significant candidates for repeat bursts were found in these ASKAP observations exceeding a threshold S/N of 10. The ASKAP detection system in the incoherent sum mode is sensitive to a fluence of 3.7 Jy ms for a nominal pulse width of 1 ms using the entire array of 36 antennas. Although, for most of the follow-up observations, smaller sub-arrays were used consisting of 23–26 antennas. Assuming a Poissonian rate distribution, we set a 95% upper limit on the burst repetition rate to be $\sim 2.4 \times 10^{-2} \text{ hr}^{-1}$ for ASKAP observations. We note here that in some repeating FRB sources, the burst rate has been found to show significant variations with time as well as frequency (Cruces et al. 2021; Xu et al. 2022; Dai et al. 2022), and so this upper limit is just a rough estimate for repetition.

5. DISCUSSION

5.1. Comparison with FRB host population

FRB 20210117A is the *only* published burst discovered in a dwarf galaxy where the repeating nature has not yet been established. We compare this source with the published sample of FRB hosts, particularly with

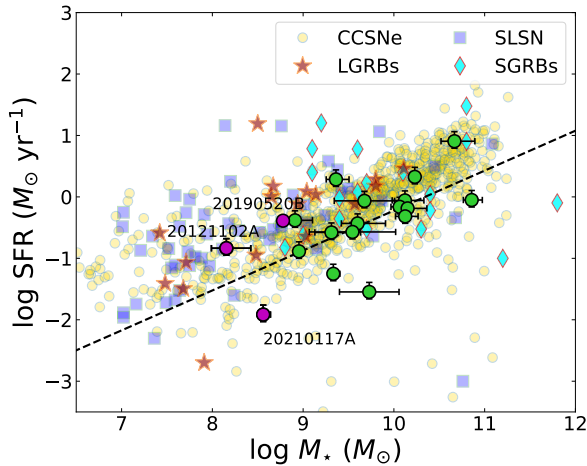


Figure 8. Stellar mass and SFR distribution for FRB hosts compared hosts of other transients. FRB dwarf host galaxies are shown in magneta, while other FRB hosts are shown in green. The hosts of CCSNe (yellow circle), SLSNe (blue squares), SGRBs (cyan diamonds), and LGRBs (red stars) are overplotted. Dashed line separates the star-forming and quiescent galaxies. The data for transients is taken from Taggart & Perley (2021), Schulze et al. (2020) and Nugent et al. (2022).

FRB 2021102A and FRB 20190520B, which are known to originate in dwarf galaxies. Despite the large excess host DM, the local environment of FRB 20210117A differs from those of FRB 2021102A and FRB 20190520B due to the lack of a PRS and a low rotation measure which is suggestive of low magnetic fields or an older system (see Table 2).

We note that FRB 20210117A has the second highest excess DM in the sample of ASKAP-localized bursts after FRB 20220610A. Simha et al. (in prep.) also studied the matter density distribution along the FRB sightline and discovered no foreground galaxies or haloes to explain the excess DM. Their study leveraged the spectroscopic redshifts of field galaxies from the FLIMFLAM survey (see Lee et al. (2022)) to model the foreground gas distribution from intervening galactic halos and also searched for possible galaxy groups whose inter-group medium might contribute to the DM. The resulting empirical model of foreground plasma indicates a very small contribution ($< 10 \text{ pc cm}^{-3}$) to the DM and thus indicates a high host galaxy or progenitor environment value.

We also search for any possible relationship between the scattering and excess DM for a sample of FRBs including FRB 20220610A ($\tau_{1 \text{ GHz}} = 0.89 \text{ ms}$) (Ryder et al. 2022) and those presented in Table 2. Except for FRB 2021102A, the scattering timescales for FRBs in this sample exceed the expectations from the ISM in

our galaxy, implying that scattering originates far beyond the Milky Way, possibly in the FRB host galaxy. We also do not find any correlation between scattering timescale and excess host DM estimates.

In Figure 8, we compare the stellar mass and SFR of FRB 20210117A’s host with the FRB host population and discover that the host has a very low SFR compared to the population. It is evident that 1) there is little ongoing star formation and no bursts of star formation in the past and, 2) the host DM constraints from $H\alpha$ measurements rule out excess DM contribution from the host, implying that the majority of the observed excess DM must come from the immediate surroundings of the FRB source. In the same figure, we also compare the stellar mass and SFRs with the hosts of other transients such as core collapse supernovae (CCSNe) (Schulze et al. 2020), superluminous supernovae (SLSNe) (Taggart & Perley 2021), and long and short GRBs (Taggart & Perley 2021; Nugent et al. 2022). Unlike dwarf hosts of repeating FRBs, the properties of FRB 20210117A hosts do not match those of SLSNe and LGRB hosts. Furthermore, unlike hosts of other ASKAP-localized FRBs, host of FRB 20210117A does not share the same space as the majority of SGRB hosts. However, it is broadly consistent with CCSNe hosts.

5.2. Potential progenitor channel

The large DM_{host} of FRB 20210117A strongly hints at the existence of a compact nebula surrounding the FRB engine. Such sources could be powered, for instance, by young pulsars in supernova remnants (Piro 2016; Connor et al. 2016), or interactions of strong winds from a young magnetar with the surrounding medium to form a pulsar wind nebula (Dai et al. 2017; Margalit & Metzger 2018). The recently proposed scenario whereby the FRB source is embedded within the powerful baryon-rich outflows from a hyper-accreting black hole (‘hypernebula’; Sridhar & Metzger 2022; Sridhar et al. 2022) could explain various properties of FRB 20210117A, including its large DM_{host} . We further investigate this model in light of our observations.

The derived isotropic-equivalent luminosity of the burst seen from FRB 20210117A is $L_{\text{FRB}} = 1.36_{-0.34}^{+1.06} \times 10^{43} \text{ erg s}^{-1}$. This requires a minimum accretion rate of $\dot{m} = \dot{M}/\dot{M}_{\text{Edd}} \gtrsim 10^6$ for the FRB to be accretion-jet powered (Sridhar et al. 2021), where \dot{M}_{Edd} is the Eddington mass transfer rate for an accreting $10M_{\odot}$ black hole. Such accretion-jet powered scenario could give rise to repeating, and potentially, even periodically active FRBs, where the periodicity may be associated with the Lens-Thirring precession timescale of the accretion disk/jet passing along the observers’ line of sight. The

Table 2. Observed properties of FRB 20210117A along with that of two active repeating FRBs localized to dwarf galaxies. The burst rate for 20121102A is the peak rate at 1.25 GHz above a fluence of 0.0015 Jy ms and $R = 1.2 \text{ GHz} (> 9.3 \text{ mJy ms})$ for 20190520B. We quote the radio luminosities for the PRS at 5 GHz. The properties of FRB 20211102A are taken from Li et al. (2021); Michilli et al. (2018); Tendulkar et al. (2017); Chatterjee et al. (2017); Marcote et al. (2017); Hessels et al. (2019) and those for FRB 20190520B are taken from Niu et al. (2022); Dai et al. (2022); Anna-Thomas et al. (2022)

FRB	z	Repeat rate (hr^{-1})	RM (rad m^{-2})	PRS luminosity (W Hz^{-1})	Host DM (pc cm^{-3})	Scattering ($\tau_{1 \text{ GHz}}$) (ms)	Pulse morphology
20121102A	0.192	122	10^5	1.4×10^{22}	≤ 324	0.02	repeater-like
20190520B	0.241	$4.5^{+1.9}_{-1.5}$	$10^3 - 10^4$	2×10^{22}	903^{+72}_{-111}	24.4	repeater-like
20210117A	0.214	$< 2.4 \times 10^{-2}$	43	$< 5.3 \times 10^{21}$	~ 460	0.86	repeater-like

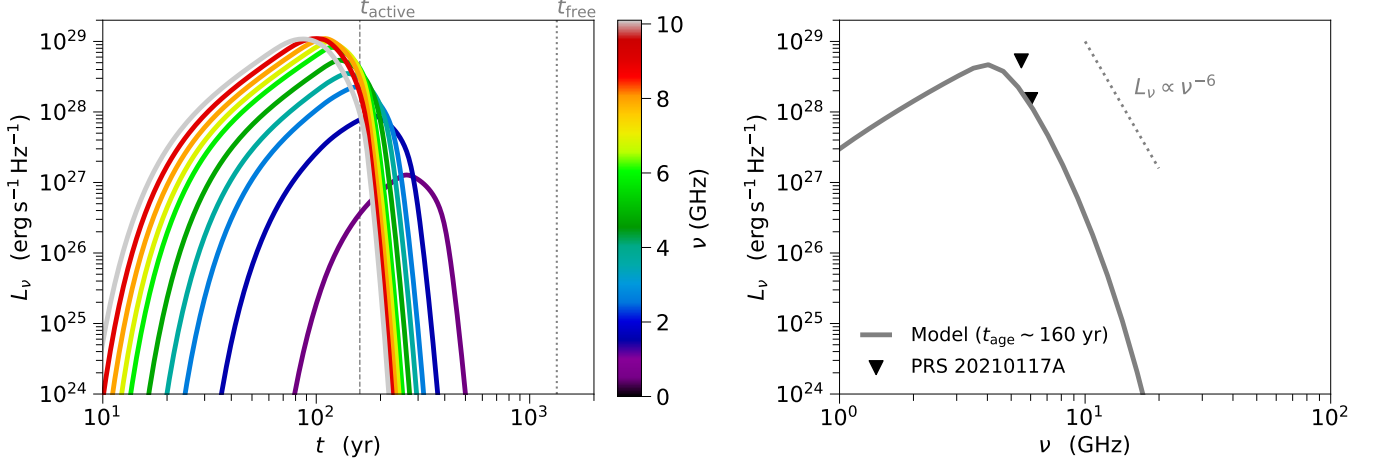


Figure 9. Radio synchrotron emission from an accretion-powered hypernebula surrounding the FRB source. Left panel: Light curves of the expanding hypernebula in different bands (color-coded). Vertical grey dashed and dotted lines denote the active duration of the central accreting engine t_{active} , and the free-expansion timescale of the hypernebula (Eq. 9), respectively (see Sec. 5.2 for more details on the system’s parameters). Right panel: Spectral energy distribution at an epoch $t_{\text{age}} = 160$ yr. Black downward-facing triangles are upper-limits of the persistent radio source (PRS) associated with FRB 20210117A.

apparent non-repetition from FRB 20210117A, in this scenario, could imply a small activity duty cycle (Sridhar et al. 2021; Katz 2021),

$$\zeta \approx \left(\frac{4f_b}{\pi^2 \theta_0^2} \right)^{1/2} \approx \frac{5}{\dot{m} \theta_0} = 5 \times 10^{-5} \left(\frac{\dot{m}}{10^6} \right)^{-1} \left(\frac{\theta_0}{0.1} \right)^{-1}, \quad (8)$$

where $f_b = 2\pi(1 - \cos(\Delta\theta))/4\pi \sim 0.01$ is the FRB beaming factor, θ_0 is the angle of the axis of jet precession, and $\Delta\theta$ is the opening angle of the jet.

The quasi-spherical disk winds, as they expand, drive a forward shock into the circumstellar medium with a typical density of say, $n \approx 10 \text{ cm}^{-3}$. On the other hand, the faster jet interacts with the slower disk winds via a termination shock. Following Sridhar & Metzger (2022), we calculate the observable properties of the hypernebula due to these interactions for the following physical parameters: velocity of the slower disk wind $v_w = 0.01 c$, velocity of the fast wind/jet $v_j = 0.1 c$, jet magnetization parameter (ratio of the magnetic energy density to the plasma rest mass energy density) $\sigma_j = 0.1$, ratio of the

wind luminosity to the jet luminosity $\eta = 0.1$, fraction of the shock power that goes into heating the electrons $\varepsilon_e = 0.5$, mass of the accreting black hole $M_\bullet = 10 M_\odot$, and mass of the companion accretor star $M_\star = 30 M_\odot$. The free expansion timescale of the outflowing winds (before they start to decelerate) is,

$$t_{\text{free}} \approx 1.3 \times 10^3 \text{ yr} \left(\frac{L_{w,42}}{n_1} \right)^{1/2} \left(\frac{v_w}{0.01 c} \right)^{-2.5}. \quad (9)$$

Above, we adopt the short-hand notation, $Y_x \equiv Y/10^x$ for quantities in cgs units.

During the free-expansion phase, the ionized wind shell contributes to a dispersion measure through it given by (Sridhar & Metzger 2022),

$$\text{DM}_{\text{sh}} \simeq 470 \text{ pc cm}^{-3} \left(\frac{\dot{m}}{10^6} \right) \left(\frac{v_w}{0.01 c} \right)^{-2} \left(\frac{t_{\text{age}}}{160 \text{ yr}} \right)^{-1}. \quad (10)$$

The model prediction of $\text{DM}_{\text{sh}} \simeq 470 \text{ pc cm}^{-3}$ is consistent with the observed $\text{DM}_{\text{host}} \sim 460 \text{ pc cm}^{-3}$ for our

chosen set of parameters. For the same set of parameters, the left panel of Fig. 9 shows the model light curves in different bands (0.1–10 GHz). Also indicated there are the active duration of the engine $t_{\text{active}} \approx M_*/\dot{M} \simeq 150$ yr, and t_{free} . Shown in the right panel of Fig. 9 is the model spectrum of the radio synchrotron emission from the shock-heated electrons, calculated when the age of the hypernebula is $t_{\text{age}} \sim 160$ yr (expansion timescale)—corresponding to the time when the model DM_{sh} tentatively matches the observed DM_{host} . We note here that the model spectrum calculated at this time of expansion is also in agreement with the upper limits on the observed persistent radio emission from FRB 20210117A.

The absolute maximum rotation measure through the nebula at time $t_{\text{age}} \sim 160$ yr is $|\text{RM}|_{\text{max}} \simeq 2 \times 10^7 \text{ rad m}^{-2}$ (Eq. 50 of Sridhar & Metzger 2022). The observed RM of $\sim 40 \text{ rad m}^{-2}$ is thus consistent within this model and could mean that the FRB was observed during a phase of RM sign reversal, as known to be seen from other FRBs too (Anna-Thomas et al. 2022; Mckinven et al. 2022; Dai et al. 2022). Such RM swings could be due to fluctuating orientations of local magnetic field lines in the turbulent eddies downstream of the termination shock, as can be expected from accreting BH outflows (e.g., Eq. 51 of Sridhar & Metzger 2022; see also Yang et al. 2022). Future long-term, short-cadence observations will reveal the trend of $|\text{RM}|_{\text{max}}$ and allow us to constrain the model parameters better to consistently explain the observed $\text{RM}(t)$ as well as the spectra.

6. SUMMARY

We have presented the discovery and sub-arcsecond localization of an apparently one-off FRB 20210117A which originates in a dwarf galaxy at a $z = 0.214$. The dwarf host galaxy has a little ongoing starformation as compared to the known dwarf host of repeating FRBs. FRB 20210117A is among the sample of FRBs with an excess host DM contribution ($\text{DM}_{\text{host}} \sim 460 \text{ pc cm}^{-3}$), where the excess DM is more likely to come from the burst’s local environment. The burst is highly (90%) linearly polarised, has a low rotation measure ($\text{RM} = 43 \text{ rad m}^{-2}$) and a flat polarisation position angle. A high time resolution analysis of FRB 20210117A and its dynamic spectrum reveals that the burst has three components and a hint of frequency drifting. While none of these characteristics are inconsistent with a non-repeating origin, flat polarization position angles and frequency drifting in particular are more commonly found in repeating sources; however, subsequent observations have not detected any repeat bursts. Moreover, we find no radio emission (either a PRS or from star formation) in our follow-up observations. Thus, the local

environment of FRB 20210117A is very different from repeating FRBs 20121102A and 20190520B with a dwarf host galaxy. Finally, we find that accretion-jet powered hypernebula model for FRB 20210117A matches with our observations.

We encourage follow-up observations to search for repeating pulses. The discovery of a repeating burst from FRB 20210117A would contradict the observed correlation between FRBs originating in dwarf galaxies and their association with a PRS.

SB would like to thank Elizabeth A. K. Adams, Reynier Peletier, Jason Hessels and the Astroflash group for useful discussions. SB is supported by a Dutch Research Council (NWO) Veni Fellowship (VI.Veni.212.058). J.X.P. as a member of the Fast and Fortunate for FRB Follow-up team, acknowledge support from NSF grants AST-1911140, AST-1910471 and AST-2206490. K.W.B., J.P.M, and R.M.S. acknowledge Australian Research Council (ARC) grant DP180100857. RMS acknowledges support through Australian Research Council Future Fellowship FT190100155 and Discovery Project DP220102305. T.E. is supported by NASA through the NASA Hubble Fellowship grant HST-HF2-51504.001-A awarded by the Space Telescope Science Institute, which is operated by the Association of Universities for Research in Astronomy, Inc., for NASA, under contract NAS5-26555. N.S. acknowledges support from NASA (grant number 80NSSC22K0332), NASA FINESST (grant number 80NSSC22K1597), and Columbia University Dean’s fellowship. C.W.J. and M.G. acknowledge support by the Australian Government through the Australian Research Council’s Discovery Projects funding scheme (project DP210102103). W.F. and A.C.G. acknowledge support by the National Science Foundation under CAREER grant No. AST-2047919, and by the David and Lucile Packard Foundation.

Based on observations collected at the European Southern Observatory under ESO programme 0105.A-0687. The Australian Square Kilometre Array Pathfinder is a part of the Australia Telescope National Facility which is managed by CSIRO. Operation of ASKAP is funded by the Australian Government with support from the National Collaborative Research Infrastructure Strategy. ASKAP uses the resources of the Pawsey Supercomputing Centre. Establishment of ASKAP, the Murchison Radio-astronomy Observatory and the Pawsey Supercomputing Centre are initiatives of the Australian Government, with support from the Government of Western Australia and the Science and Industry Endowment Fund. We acknowledge the Wa-

jarri Yamatji as the traditional owners of the Murchison Radio-astronomy Observatory site. The Australia Telescope Compact Array is part of the Australia Telescope National Facility which is funded by the Australian Government for operation as a National Facility managed by CSIRO. We acknowledge the Gomeri people as the traditional owners of the Observatory site. The National Radio Astronomy Observatory is a facility of the National Science Foundation operated under cooperative agreement by Associated Universities, Inc. Some of the data presented herein were obtained at the W. M. Keck Observatory, which is operated as a scientific partnership among the California Institute of Technology, the University of California and the National Aeronautics and Space Administration. The Observatory was made possible by the generous financial support of the W. M. Keck Foundation. W. M. Keck Observatory access was supported by Northwestern University and the Center

for Interdisciplinary Exploration and Research in Astrophysics (CIERA). The authors wish to recognize and acknowledge the very significant cultural role and reverence that the summit of Maunakea has always had within the indigenous Hawaiian community. We are most fortunate to have the opportunity to conduct observations from this mountain.

Facilities: ASKAP, VLA, ATCA, VLT (HAWK-I, FOR2), Keck.

Software: astropy (Astropy Collaboration et al. 2013, 2018), numpy (Harris et al. 2020), matplotlib (Hunter 2007), lmfit (Newville et al. 2016), PyMultiNest (Buchner et al. 2014), bilby (Ashton et al. 2019), fetch (Agarwal et al. 2020), PSRCHIVE (van Straten et al. 2012), miriad (Sault et al. 1995), CASA (McMullin et al. 2007).

REFERENCES

- Agarwal, D., Aggarwal, K., Burke-Spolaor, S., Lorimer, D. R., & Garver-Daniels, N. 2020, MNRAS, 497, 1661
- Aggarwal, K., Budavári, T., Deller, A. T., et al. 2021, ApJ, 911, 95
- Amiri, M., Andersen, B. C., Bandura, K., et al. 2021, ApJS, 257, 59
- Anna-Thomas, R., Connor, L., Burke-Spolaor, S., et al. 2022, arXiv e-prints, arXiv:2202.11112
- Ashton, G., Hübner, M., Lasky, P. D., et al. 2019, ApJS, 241, 27
- Astropy Collaboration, Robitaille, T. P., Tollerud, E. J., et al. 2013, A&A, 558, A33
- Astropy Collaboration, Price-Whelan, A. M., Sipőcz, B. M., et al. 2018, AJ, 156, 123
- Barsdell, B. R. 2012, PhD thesis, Swinburne University of Technology
- Berriman, G. B., & Good, J. C. 2017, Publications of the Astronomical Society of the Pacific, 129, 058006
- Bhandari, S., Sadler, E. M., Prochaska, J. X., et al. 2020, ApJL, 895, L37
- Bhandari, S., Heintz, K. E., Aggarwal, K., et al. 2022, AJ, 163, 69
- Buchner, J., Georgakakis, A., Nandra, K., et al. 2014, A&A, 564, A125
- Calzetti, D. 2001, PASP, 113, 1449
- Chatterjee, S., Law, C. J., Wharton, R. S., et al. 2017, Nature, 541, 58
- Chen, G., Ravi, V., & Hallinan, G. W. 2022, arXiv e-prints, arXiv:2201.00999
- Cho, H., Macquart, J.-P., Shannon, R. M., et al. 2020, ApJL, 891, L38
- Connor, L., Sievers, J., & Pen, U.-L. 2016, MNRAS, 458, L19
- Conroy, C. 2013, ARA&A, 51, 393
- Conroy, C., & Gunn, J. E. 2010, ApJ, 712, 833
- Conroy, C., Gunn, J. E., & White, M. 2009, ApJ, 699, 486
- Cordes, J. M., & Lazio, T. J. W. 2002, arXiv e-prints, arXiv:0207156
- Cruces, M., Spitler, L. G., Scholz, P., et al. 2021, MNRAS, 500, 448
- Dai, S., Feng, Y., Yang, Y. P., et al. 2022, arXiv e-prints, arXiv:2203.08151
- Dai, Z. G., Wang, J. S., & Yu, Y. W. 2017, ApJL, 838, L7
- Day, C. K., Deller, A. T., James, C. W., et al. 2021, PASA, 38, e050
- Day, C. K., Deller, A. T., Shannon, R. M., et al. 2020, MNRAS, 497, 3335
- Drlica-Wagner, A., Ferguson, P. S., Adamów, M., et al. 2022, The Astrophysical Journal Supplement Series, 261, 38
- Fong, W.-f., Dong, Y., Leja, J., et al. 2021, ApJL, 919, L23
- Freudling, W., Romaniello, M., Bramich, D. M., et al. 2013, A&A, 559, 96
- Gallazzi, A., Charlot, S., Brinchmann, J., White, S. D. M., & Tremonti, C. A. 2005, MNRAS, 362, 41
- Harris, C. R., Millman, K. J., van der Walt, S. J., et al. 2020, Nature, 585, 357
- Heintz, K. E., Prochaska, J. X., Simha, S., et al. 2020, arXiv e-prints, arXiv:2009.10747

- Hessels, J. W. T., Spitler, L. G., Seymour, A. D., et al. 2019, *Astrophys. J.*, 876, L23
- Hilmarsson, G. H., Michilli, D., Spitler, L. G., et al. 2021, *ApJL*, 908, L10
- Hunter, J. D. 2007, *Computing in Science and Engineering*, 9, 90
- James, C. W., Prochaska, J. X., Macquart, J. P., et al. 2022a, *MNRAS*, 509, 4775
- James, C. W., Ghosh, E. M., Prochaska, J. X., et al. 2022b, *MNRAS*, 516, 4862
- James, P. A., Shane, N. S., Beckman, J. E., et al. 2004, *A&A*, 414, 23
- Johnson, B. D., Leja, J., Conroy, C., & Speagle, J. S. 2021, *ApJS*, 254, 22
- Kaisin, S. S., Karachentsev, I. D., & Ravindranath, S. 2012, *MNRAS*, 425, 2083
- Katz, J. I. 2021, *MNRAS*, 502, 4664
- Kirsten, F., Marcote, B., Nimmo, K., et al. 2022, *Nature*, 602, 585
- Kriek, M., & Conroy, C. 2013, *ApJL*, 775, L16
- Kroupa, P. 2001, *MNRAS*, 322, 231
- Kumar, P., Shannon, R. M., Flynn, C., et al. 2021, *MNRAS*, 500, 2525
- Lang, D., Hogg, D. W., Mierle, K., Blanton, M., & Roweis, S. 2010, *ApJ*, 139, 1782
- Lee, K.-G., Ata, M., Khrykin, I. S., et al. 2022, *ApJ*, 928, 9
- Leja, J., Carnall, A. C., Johnson, B. D., Conroy, C., & Speagle, J. S. 2019, *ApJ*, 876, 3
- Li, D., Wang, P., Zhu, W. W., et al. 2021, *Nature*, 598, 267
- Lindgren, L., Hernández, J., Bombrun, A., et al. 2018, *A&A*, 616, A2
- Macquart, J.-P., Shannon, R. M., Bannister, K. W., et al. 2019, *ApJL*, 872, L19
- Macquart, J. P., Prochaska, J. X., McQuinn, M., et al. 2020, *Nature*, 581, 391
- Marcote, B., Paragi, Z., Hessels, J. W. T., et al. 2017, *ApJL*, 834, L8
- Marcote, B., Nimmo, K., Hessels, J. W. T., et al. 2020, *Nature*, 577, 190
- Margalit, B., Berger, E., & Metzger, B. D. 2019, *ApJ*, 886, 110
- Margalit, B., & Metzger, B. D. 2018, *ApJL*, 868, L4
- Marnoch, L., Ryder, S. D., Bannister, K. W., et al. 2020, *A&A*, 639, A119
- McConnell, D., Hale, C. L., Lenc, E., et al. 2020, *PASA*, 37, e048
- Mckinven, R., Gaensler, B. M., Michilli, D., et al. 2022, *arXiv e-prints*, arXiv:2205.09221
- McMullin, J. P., Waters, B., Schiebel, D., Young, W., & Golap, K. 2007, in *Astronomical Society of the Pacific Conference Series*, Vol. 376, *Astronomical Data Analysis Software and Systems XVI*, ed. R. A. Shaw, F. Hill, & D. J. Bell, 127
- Michilli, D., Seymour, A., Hessels, J. W. T., et al. 2018, *Nature*, 553, 182
- Newville, M., Stensitzki, T., Allen, D. B., et al. 2016, *Lmfit: Non-Linear Least-Square Minimization and Curve-Fitting for Python*, *Astrophysics Source Code Library*, , ascl:1606.014
- Niu, C. H., Aggarwal, K., Li, D., et al. 2022, *Nature*, 606, 873
- Nugent, A. E., Fong, W.-f., Dong, Y., et al. 2022, *arXiv e-prints*, arXiv:2206.01764
- Petroff, E., Barr, E. D., Jameson, A., et al. 2016, *PASA*, 33, e045
- Piro, A. L. 2016, *ApJL*, 824, L32
- Pleunis, Z., Good, D. C., Kaspi, V. M., et al. 2021, *ApJ*, 923, 1
- Prochaska, J., Hennawi, J., Westfall, K., et al. 2020, *The Journal of Open Source Software*, 5, 2308
- Prochaska, J. X., & Zheng, Y. 2019, *MNRAS*, 485, 648
- Qiu, H., Shannon, R. M., Farah, W., et al. 2020, *MNRAS*, arXiv:2006.16502
- Ravi, V., Catha, M., Addario, L. D., et al. 2019, *Nature*, doi:10.1038/s41586-019-1389-7
- Ravi, V., Catha, M., Chen, G., et al. 2022, *arXiv e-prints*, arXiv:2211.09049
- Ryder, S. D., Bannister, K. W., Bhandari, S., et al. 2022, *arXiv e-prints*, arXiv:2210.04680
- Salpeter, E. E. 1966, *AJ*, 71, 869
- Sault, R. J., Teuben, P. J., & Wright, M. C. H. 1995, in *Astronomical Society of the Pacific Conference Series*, Vol. 77, *Astronomical Data Analysis Software and Systems IV*, ed. R. A. Shaw, H. E. Payne, & J. J. E. Hayes, 433
- Schulze, S., Yaron, O., Sollerman, J., et al. 2020, *arXiv e-prints*, arXiv:2008.05988
- Shannon, R. M., Macquart, J.-P., Bannister, K. W., et al. 2018, *Nature*, 562, 386
- Skrutskie, M. F., Cutri, R. M., Stiening, R., et al. 2006, *The Astronomical Journal*, 131, 1163
- Speagle, J. S. 2020, *MNRAS*, 493, 3132
- Spitler, L. G., Scholz, P., Hessels, J. W. T., et al. 2016, *Nature*, 531, 202
- Sridhar, N., & Metzger, B. D. 2022, *ApJ*, 937, 5
- Sridhar, N., Metzger, B. D., Beniamini, P., et al. 2021, *ApJ*, 917, 13

- Sridhar, N., Metzger, B. D., & Fang, K. 2022, arXiv e-prints, arXiv:2212.11236
- Sutinjo, A. T., Scott, D. R., James, C. W., et al. 2023, arXiv e-prints, arXiv:2302.06220
- Taggart, K., & Perley, D. A. 2021, MNRAS, 503, 3931
- Tendulkar, S. P., Bassa, C. G., Cordes, J. M., et al. 2017, ApJL, 834, L7
- van Straten, W., Demorest, P., & Osłowski, S. 2012, Astronomical Research and Technology, 9, 237
- Xu, H., Niu, J. R., Chen, P., et al. 2022, Nature, 609, 685
- Xu, J., & Han, J. L. 2015, Research in A&A, 15, 1629
- Yang, Y.-P., Xu, S., & Zhang, B. 2022, arXiv e-prints, arXiv:2208.08712
- Yao, J. M., Manchester, R. N., & Wang, N. 2017, ApJ, 835, 29